Supporting Information

for

Chloride-induced steel corrosion in alkali-activated fly ash mortar: increased propensity for corrosion initiation at defects

Gregor J. G. Gluth*, Gino Ebell, Petr Hlaváček, Jürgen Mietz

Bundesanstalt für Materialforschung und -prüfung (BAM), Berlin, Germany

* Corresponding author; e-mail: gregor.gluth@bam.de

(published in *Materials and Corrosion* 2020)

This file includes:

Figures S1 to S30

Table S1

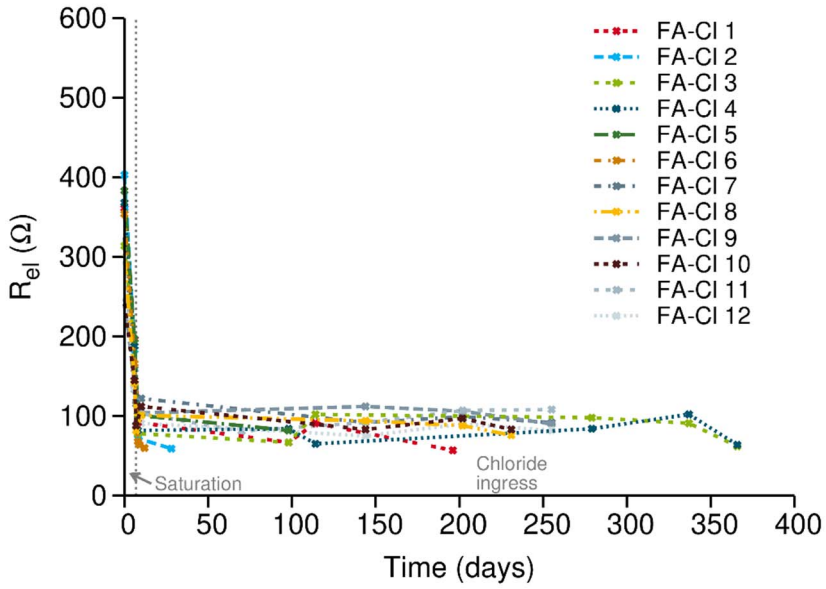

Figure S1. Evolution of the ohmic resistance (R_{el}) of the alkali-activated fly ash mortar exposed to chloride ("Cl").

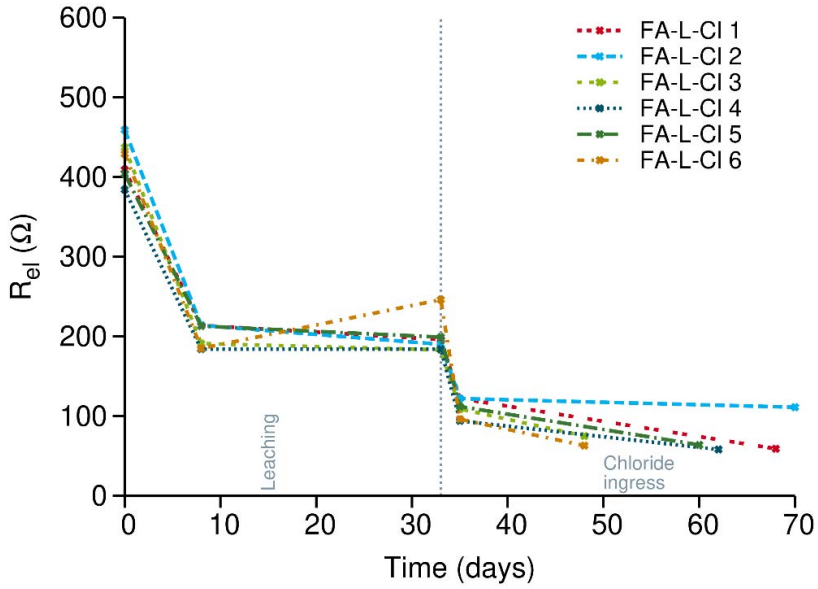

Figure S2. Evolution of the ohmic resistance (R_{el}) of the alkali-activated fly ash mortar exposed to leaching and chloride ("L-Cl").

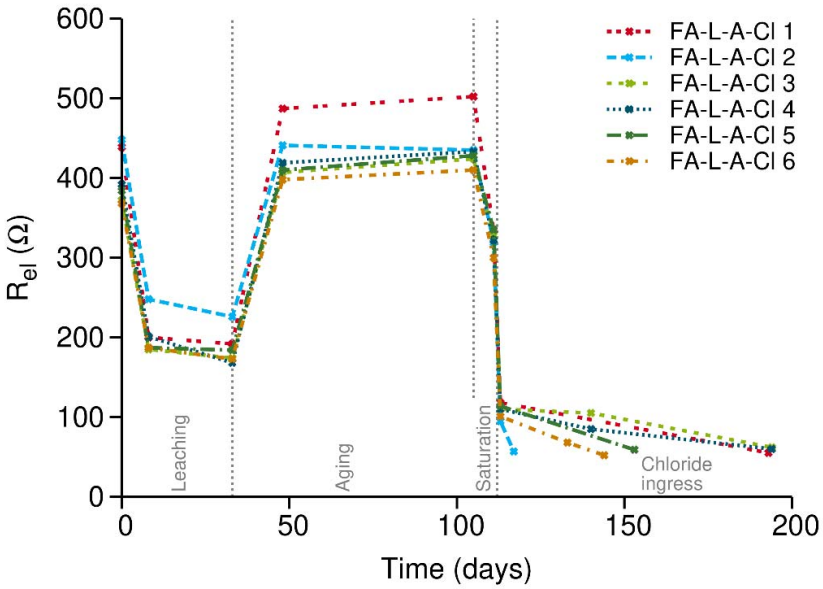

Figure S3. Evolution of the ohmic resistance (R_{el}) of the alkali-activated fly ash mortar exposed to leaching, aging and chloride ("L-A-Cl").

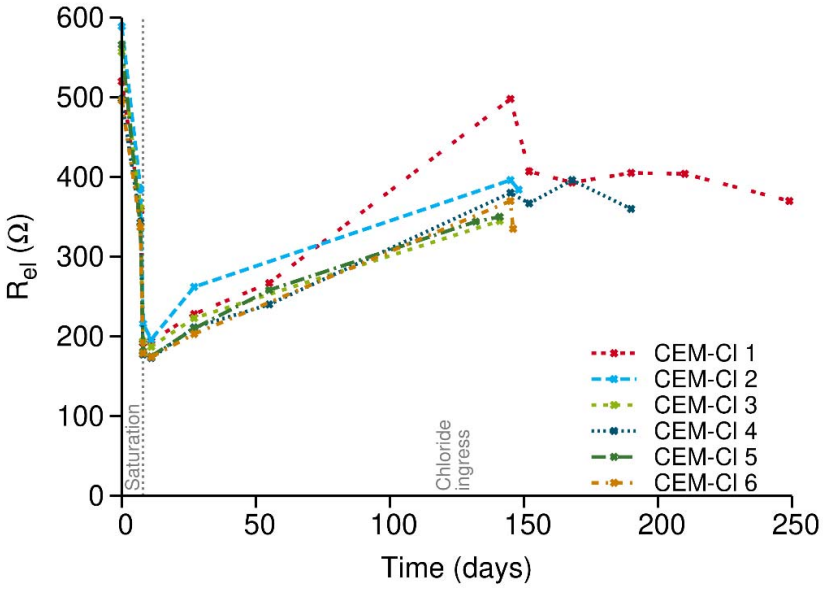

Figure S4. Evolution of the ohmic resistance (R_{el}) of the Portland cement mortar exposed to chloride ("Cl").

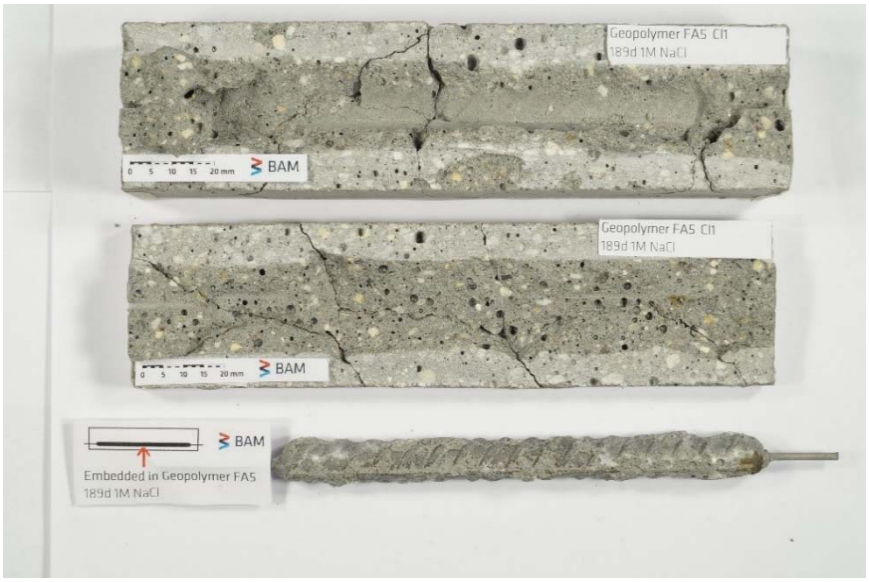

Figure S5. Mortar specimen FA-Cl 1 and embedded steel rebar split after depassivation of the steel was detected.

Figure S6. Mortar specimen FA-Cl 2 and embedded steel rebar split after depassivation of the steel was detected.

Figure S7. Mortar specimen FA-Cl 3 and embedded steel rebar split after depassivation of the steel was detected.

Figure S8. Mortar specimen FA-Cl 4 and embedded steel rebar split after depassivation of the steel was detected.

Figure S9. Mortar specimen FA-Cl 6 and embedded steel rebar split after depassivation of the steel was detected.

Figure S10. Mortar specimen FA-Cl 8 and embedded steel rebar split after depassivation of the steel was detected.

Figure S11. Mortar specimen FA-Cl 10 and embedded steel rebar split after depassivation of the steel was detected.

Figure S12. Mortar specimen FA-L-Cl 1 and embedded steel rebar split after depassivation of the steel was detected.

Figure S13. Mortar specimen FA-L-Cl 3 and embedded steel rebar split after depassivation of the steel was detected.

Figure S14. Mortar specimen FA-L-Cl 4 and embedded steel rebar split after depassivation of the steel was detected.

Figure S15. Mortar specimen FA-L-Cl 5 and embedded steel rebar split after depassivation of the steel was detected.

Figure S16. Mortar specimen FA-L-Cl 6 and embedded steel rebar split after depassivation of the steel was detected.

Figure S17. Mortar specimen FA-L-A-Cl 1 and embedded steel rebar split after depassivation of the steel was detected.

Figure S18. Mortar specimen FA-L-A-Cl 2 and embedded steel rebar split after depassivation of the steel was detected.

Figure S19. Mortar specimen FA-L-A-Cl 3 and embedded steel rebar split after depassivation of the steel was detected.

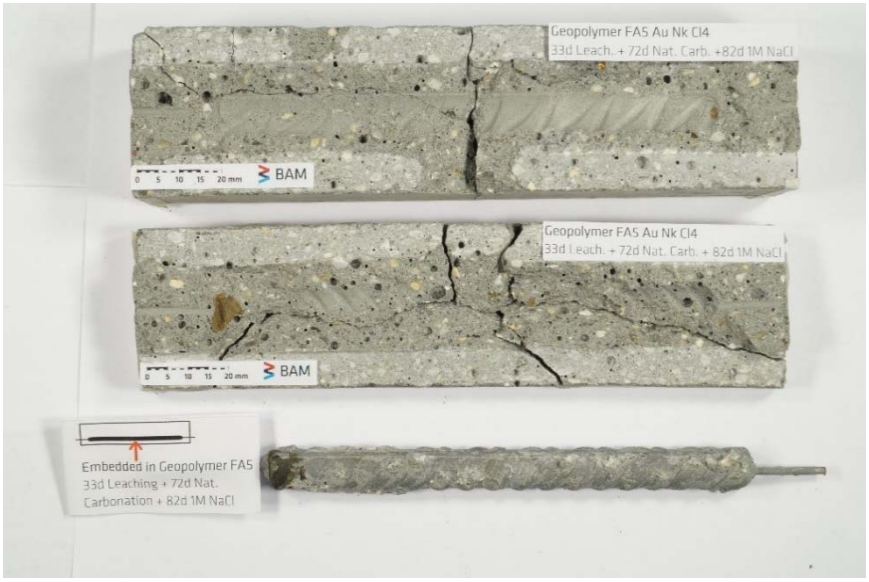

Figure S20. Mortar specimen FA-L-A-Cl 4 and embedded steel rebar split after depassivation of the steel was detected.

Figure S21. Mortar specimen FA-L-A-Cl 5 and embedded steel rebar split after depassivation of the steel was detected.

Figure S22. Mortar specimen FA-L-A-Cl 6 and embedded steel rebar split after depassivation of the steel was detected.

Figure S23. Mortar specimen CEM-Cl 1 and embedded steel rebar split after depassivation of the steel was detected.

Figure S24. Mortar specimen CEM-Cl 2 and embedded steel rebar split after depassivation of the steel was detected.

Figure S25. Mortar specimen CEM-Cl 3 and embedded steel rebar split after depassivation of the steel was detected.

Figure S26. Mortar specimen CEM-Cl 4 and embedded steel rebar split after depassivation of the steel was detected.

Figure S27. Mortar specimen CEM-Cl 5 and embedded steel rebar split after depassivation of the steel was detected.

Figure S28. Mortar specimen CEM-A-Cl 6 and embedded steel rebar split after depassivation of the steel was detected.

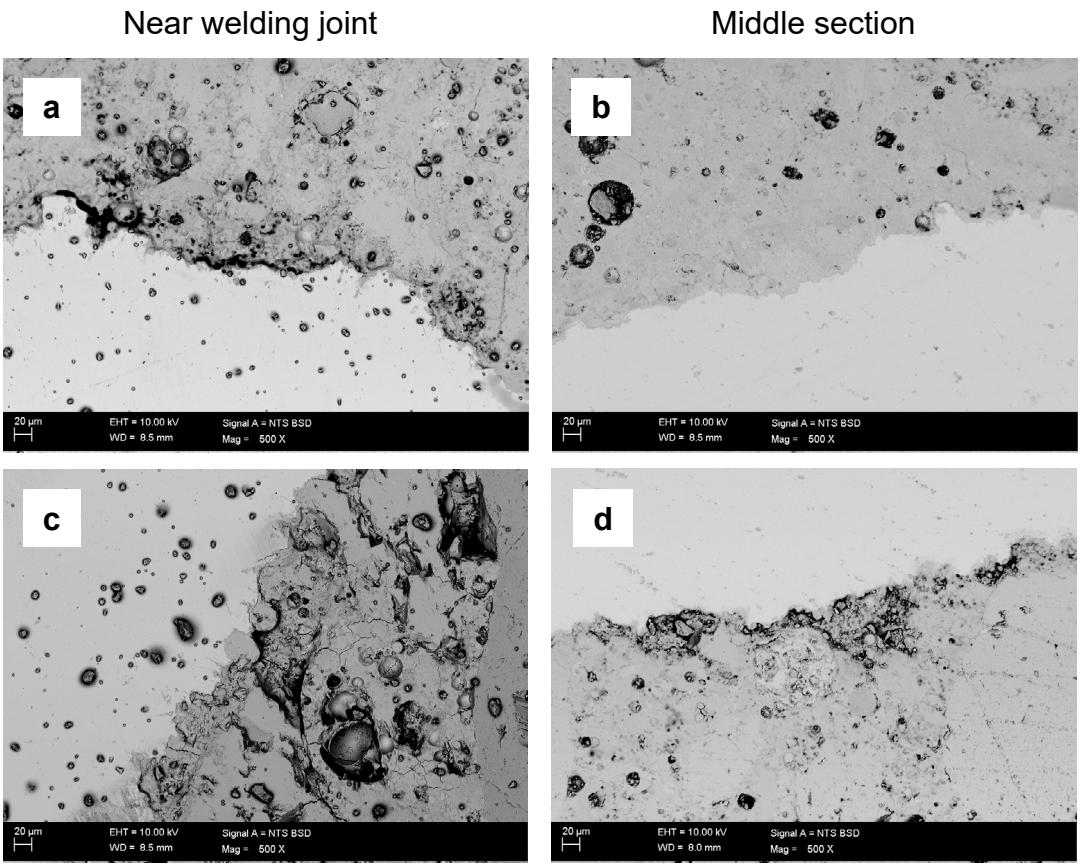

Figure S29. Scanning electron micrographs (BSE mode) of the steel-mortar interface in an alkali-activated fly ash mortar in the region close to the rebar end, *i.e.* close to a welding joint (a, c), and in the central region of the mortar prism (b, d).

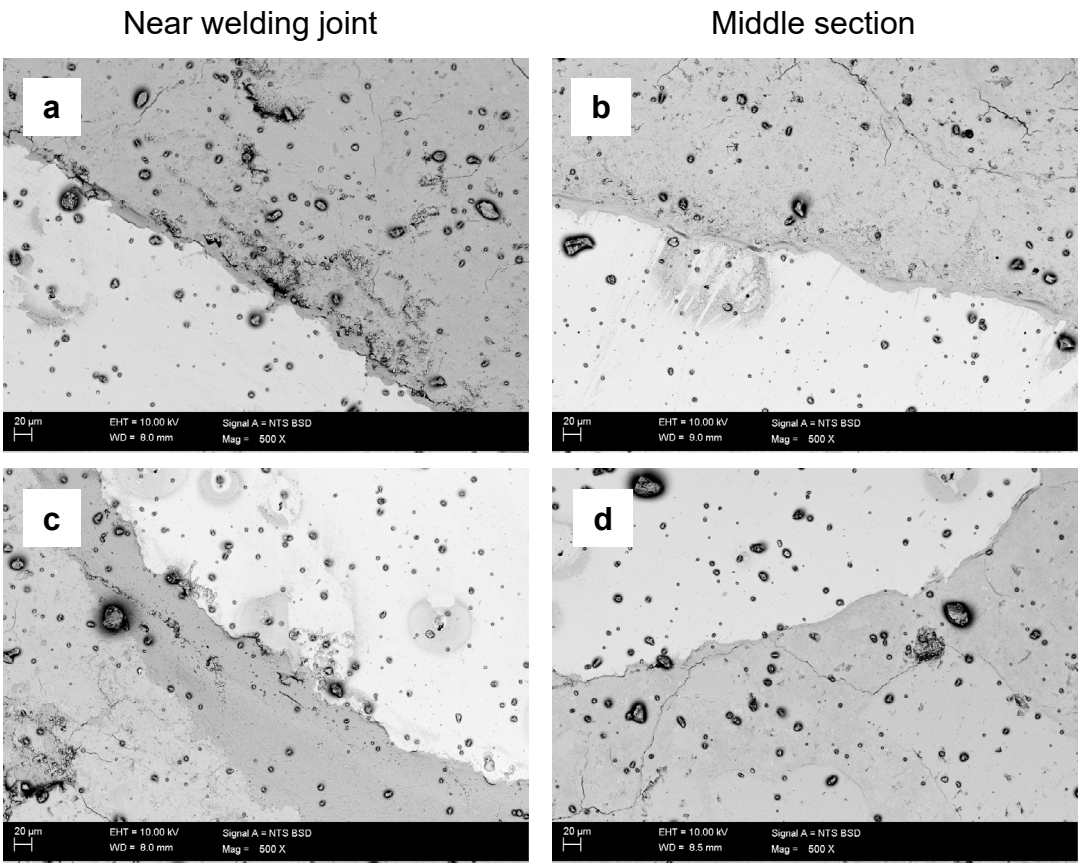

Figure S30. Scanning electron micrographs (BSE mode) of the steel-mortar interface in a Portland cement mortar in the region close to the rebar end, *i.e.* close to a welding joint (a, c), and in the central region of the mortar prism (b, d).

Table S1. Corrosion-initiating chloride contents (in wt.% wrt binder) for the individual specimens. Values of specimens in which corrosion initiation occurred adjacent to the welding joint between the steel rebar and the stainless-steel wires are marked in grey.

	Mortar/exposure conditions			
	FA-Cl	FA-L-Cl	FA-L-A-Cl	CEM-Cl
Specimen 1	0.376	0.555	0.435	2.275
Specimen 2	0.557		0.231	1.293
Specimen 3	0.711	1.140	0.388	1.124
Specimen 4	0.604	1.051	0.358	1.826
Specimen 5		0.382	0.341	0.831
Specimen 6	0.228	2.342	0.332	0.963
Specimen 8	0.548			
Specimen 10	0.512			